

An Integrated Magnetic Isolated Two-Inductor Boost Converter: Analysis, Design and Experimentation

Liang Yan, *Student Member, IEEE*, and Brad Lehman, *Member, IEEE*

Abstract—This paper presents an integrated magnetic isolated two-inductor boost converter.¹ All magnetic components are integrated into one magnetic assembly. Two inductor windings are intrinsically coupled to allow input current to increase only when both primary switches are closed. The operation principle, start-up, and protection mechanisms are detailed. A prototype converter has been built. Experimental and simulation results verify the analysis.

Index Terms—Boost converter, integrated magnetics, magnetic assembly.

I. INTRODUCTION

THE two-inductor boost converter exhibits benefits in high power applications [1]–[8]: high input current is split between two inductors, thus reducing I^2R power loss in both copper windings and primary switches. Furthermore, by applying an interleaving control strategy, the input current ripple can be reduced [3]. Implementation of the topology can be in either nonisolated [9] or isolated format [10]. The isolated boost topology, which is shown in Fig. 1 [10], is attractive in applications such as power factor correction (PFC) with isolation and battery or fuel cell powered devices to generate high output voltage from low input voltage [9]–[12].

The main obstacle of the circuit in Fig. 1 is its limited power regulation range. Inductor L_1 must support input voltage whenever Q_1 turns on. Likewise, this is true for L_2 and Q_2 . Since the minimum duty ratio of each switch is 0.5, the magnetizing currents of the two inductors cannot be limited. This leads to a minimum output power level. If the load demands less power than this minimum level, the output voltage increases abnormally because excessive energy has been stored in the inductors.

A recent solution to this limitation on minimum power is given in Fig. 2 [11], [12]. An auxiliary transformer T_2 is inserted in series with inductor L_1 and L_2 . Transformer T_2 magnetically couples two input current paths. The currents in the two inductors are then forced to be identical. Theoretically, the input current only increases when both Q_1 and Q_2 turn on. If the overlapping between two driving signals is small, the inductor currents become discontinuous. This improvement makes the

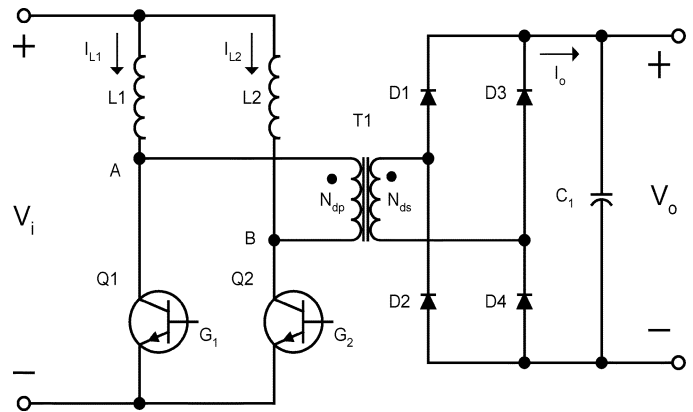


Fig. 1. Conventional two-inductor boost converter [10].

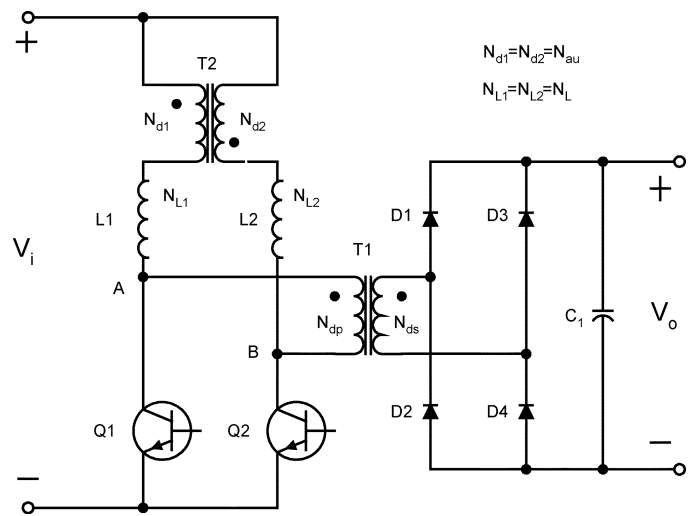


Fig. 2. Two-inductor boost converter with auxiliary transformer [11].

two-inductor boost circuit attractive in application. However, a disadvantage of the approach is that the circuit requires four magnetic components on the primary side, thus, requiring additional board space.

This paper proposes an integrated magnetic isolated two-inductor boost converter that uses only one magnetic assembly. Advantages of the topology include the properties that it does the following.

- 1) Implements the isolated two-inductor boost converter with one magnetic assembly, thereby reducing the board space.
- 2) Maintains wide power regulation range: that is, under the condition that the output voltage is regulated, the input

Manuscript received October 7, 2003; revised September 13, 2004. This paper was presented in part at the IEEE Applied Power Electronics Conference, Miami, FL, 2002. Recommended by Associate Editor J. Cobos.

L. Yan is with MKS ENI Products, Rochester, NY 14623 USA (e-mail: lian@ece.neu.edu; liang_yan@mksinst.com).

B. Lehman is with the Department of Electrical and Computer Engineering, Northeastern University, Boston, MA 02115 USA (e-mail: lehman@ece.neu.edu).

Digital Object Identifier 10.1109/TPEL.2004.843004

¹Patent pending: USPTO/Worldwide filing number 60/444821.

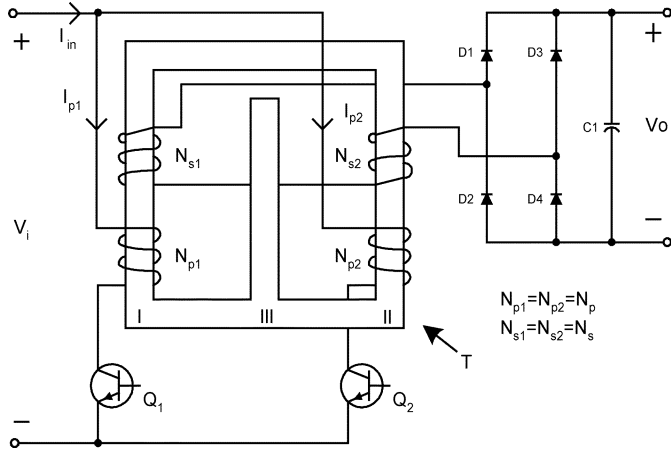


Fig. 3. Proposed integrated magnetic two-inductor boost converter.

power is limited when the overlapping of driving signals is small.

- 3) Has a reduced number of windings (two windings) on the primary side of the circuit compared to the topology in Fig. 2 (five windings). The copper loss can be reduced because of fewer windings and soldering connections.
- 4) Implements the start-up and protection windings within the same magnetic assembly without adding components to the primary circuit.

To our knowledge, this is the first time a two-inductor isolated boost converter has been proposed with integration of all magnetic components. For broad discussions of the advantages and disadvantages in general integrated magnetic technologies, the reader is referred to [13]–[16].

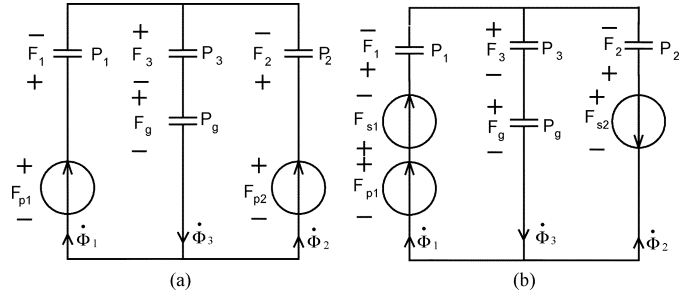
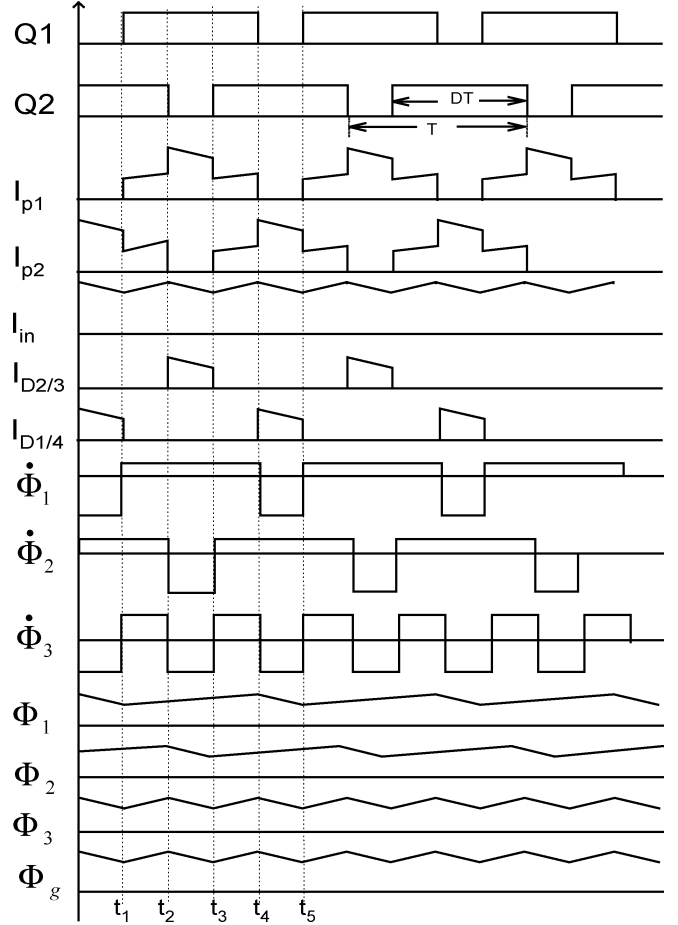
Section II proposes the integrated magnetic two-inductor boost converter. Section III presents the transformer design formulas. Section IV gives a comparison between the proposed circuit and its counterpart that uses discrete magnetic cores. Section V discusses some practical issues including start-up and protection. Section VI shows two topology variations. Section VII presents the simulation and experimental results, and Section VIII gives conclusions. In the Appendix, the derivation of formulas used in Section III is detailed.

II. PROPOSED INTEGRATED MAGNETIC TWO-INDUCTOR BOOST CONVERTER

Fig. 3 is the proposed integrated magnetic two-inductor boost converter. The transformer uses a single three-leg magnetic core with a gap in the center leg. Two inductor windings N_{p1} and N_{p2} are wound around two outer legs. Secondary windings N_{s1} and N_{s2} are wound around two outer legs correspondingly and connected in series. Since N_{p1} and N_{p2} are on the primary side and behave as primary windings, we refer to them in this paper as primary windings.

A. Operating Principle

Fig. 4 models two circuit states (according to the states of switches Q_1 and Q_2) in a half switching cycle using the capacitor modeling method [17]–[20]. In the capacitor modeling method, each current source represents an active winding and each capacitor represents a permeance. In this method


 Fig. 4. Two state models (current sources represent active windings). (a) Q_1 on and Q_2 off ($t_1 \sim t_2$ in Fig. 5). (b) Q_1 on and Q_2 off ($t_2 \sim t_3$ in Fig. 5).

 Fig. 5. Operating waveforms. Q_1, Q_2 : the driving signals of two primary switches; I_{p1} and I_{p2} : the currents in the two primary windings; I_{in} : the input current; $I_{D2/3}$: the current in diode D_2 and D_3 ; $I_{D1/4}$: the current in diode D_1 and D_4 ; $\dot{\Phi}_1 \sim \dot{\Phi}_3$: the flux rates in the core legs; $\Phi_1 \sim \Phi_3$: the fluxes in the core legs; Φ_g : the flux in the gap.

when a winding does not conduct current, its current source is represented as a short circuit. $\dot{\Phi}_j(j=1,2,3)$ are the flux rates within core legs (i.e., the derivative of flux, which is equal to V/N , where V is the voltage on the winding around the core leg and N is the number of winding turns.); $P_j(j=1,2,3)$ are the permeances of the core legs; P_g is the permeance of the gap; $F_j(j=1,2,3)$ are the magnetomotive forces (mmfs) on permeances $P_j(j=1,2,3)$; $F_{pj}(j=1,2)$ and $F_{sj}(j=1,2)$ are the mmfs on the primary and secondary windings, respectively; F_g is the mmf of the gap. Fig. 5 illustrates the operating waveforms of the proposed two-inductor boost converter. Time $t_1 \sim t_5$ is

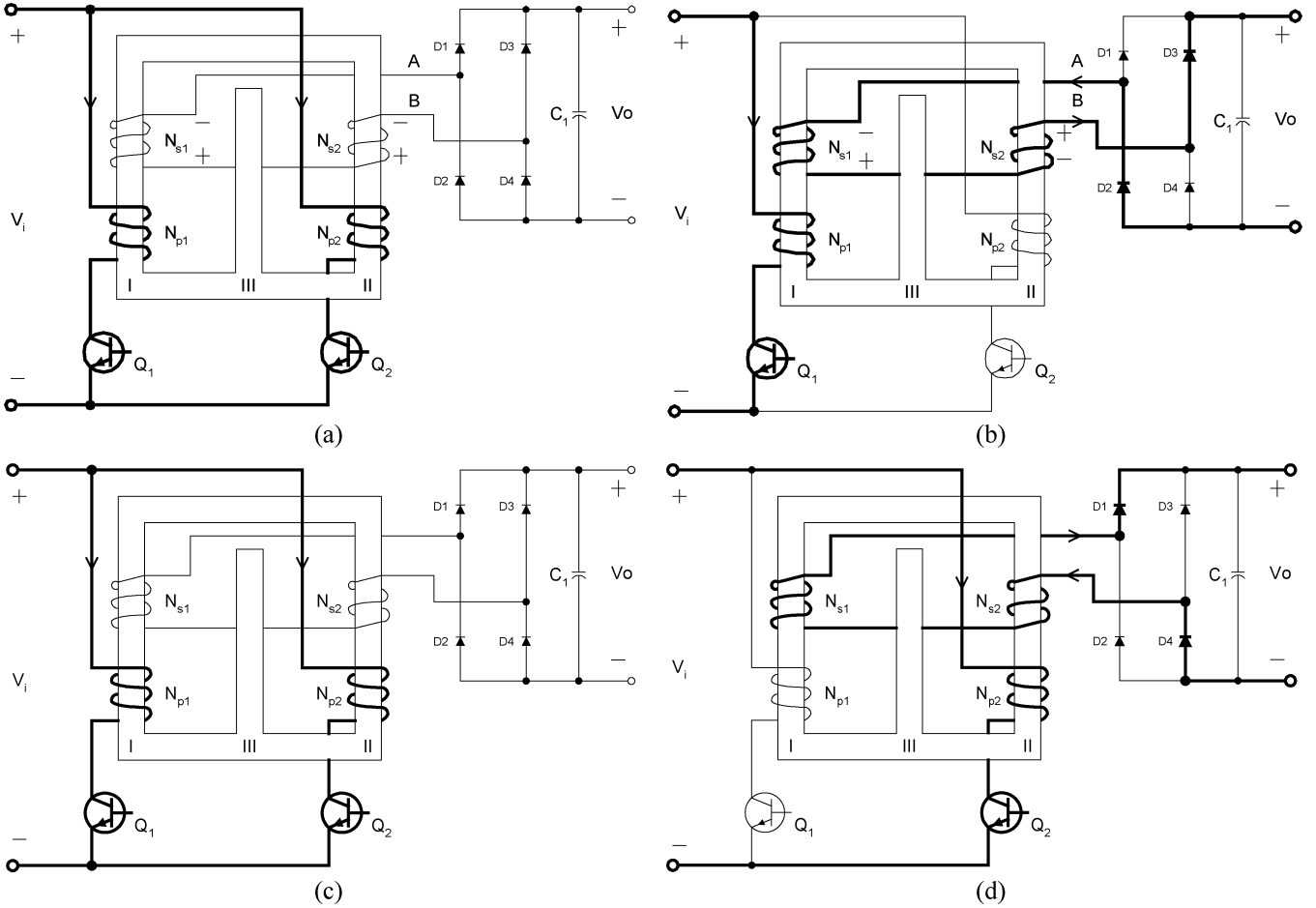


Fig. 6. Current paths. (a) $t_1 \sim t_2$. (b) $t_2 \sim t_3$. (c) $t_3 \sim t_4$. (d) $t_4 \sim t_5$.

one switching cycle, including four operating phases. Fig. 6 shows the current flowing paths in each phase. To simplify the analysis, all the devices are assumed to be ideal. The mmfs on the permeance of the core legs are neglected $F_{j(j=1,2,3)} = 0$, i.e., these permeance are assumed to be infinite compared with the permeance of the gap. Let the driving signals of Q_1 and Q_2 be as in Fig. 5. The operation principle can be explained as follows.

- 1) **Time $t_1 \sim t_2$:** At this time interval, both switches Q_1 and Q_2 turn on. The currents in the primary windings increase as I_{p1} and I_{p2} in Fig. 5. The voltages on secondary windings N_{s1} and N_{s2} are equal, but the polarities are opposite. Hence, the overall voltage difference between two output terminals [A and B in Fig. 6(a)] is zero. All diodes are blocked. The flux level (Φ_g) in the gap increases. This is the energy storage stage as in a typical boost circuit. The flux rates in the two outer legs can be determined directly from the voltages on windings N_{p1} and N_{p2}

$$\dot{\Phi}_1 = \frac{V_i}{N_{p1}}, \quad \dot{\Phi}_2 = \frac{V_i}{N_{p2}}. \quad (1)$$

By KCL in Fig. 4, the flux rate in the center leg is the summation of the flux rates in two outer legs. Let $N_{p1} = N_{p2} = N_p$, then

$$\dot{\Phi}_3 = \dot{\Phi}_1 + \dot{\Phi}_2 = \frac{2V_i}{N_p}. \quad (2)$$

Assume the flux rates have directions as marked in the models of Fig. 4. Fig. 5 shows both the flux rates and the flux in each leg. Since the voltages on the windings are constant in this stage, the flux rates in the core legs are also constant. Thus, the fluxes increase linearly.

- 2) **Time $t_2 \sim t_3$:** Switch Q_2 turns off. The current in winding N_{p2} reduces to zero. N_{p1} delivers input power to the secondary side. $I_{p1} = I_{in}$, $I_{p2} = 0$, where I_{in} is the input current. The voltages on secondary windings N_{s1} and N_{s2} forward bias D_2 and D_3 . The currents in D_2 and D_3 are shown in Fig. 5 as $I_{D2/3}$. The stored energy in the gap is released and the flux level (Φ_g) decreases. Applying the same derivation method, the flux rates are obtained

$$\dot{\Phi}_1 = \frac{V_i}{N_{p1}}, \quad \dot{\Phi}_2 = -\frac{V_o - \frac{V_i N_{s1}}{N_{p1}}}{N_{s2}}. \quad (3)$$

The actual direction of flux rate $\dot{\Phi}_2$ is downward. Use KCL in Fig. 4 and let $N_{s1} = N_{s2} = N_s$ to obtain

$$\dot{\Phi}_3 = \frac{2V_i}{N_p} - \frac{V_o}{N_s}. \quad (4)$$

The flux rates in the core legs are constant in this stage. So flux Φ_1 increases ($\dot{\Phi}_1 > 0$) and flux Φ_2 , Φ_3 decrease ($\dot{\Phi}_2 < 0$, $\dot{\Phi}_3 < 0$) linearly. The voltage on Q_2 is $\dot{\Phi}_2 N_{p2} + V_i = (N_p/N_s)V_o$. Rectifier D_1 and D_4 support voltage V_o .

- 3) **Time $t_3 \sim t_4$:** Both switches Q_1 and Q_2 turn on. This operating phase is the same as that in time interval $t_1 \sim t_2$.
- 4) **Time $t_4 \sim t_5$:** Switch Q_1 turns off. In this phase, N_{p2} delivers input power to the secondary side, while N_{p1} is disconnected from the input. D_1 and D_4 conduct output current. The voltage on Q_1 is equal to $(N_p/N_s)V_o$. The voltages on rectifiers D_2 and D_3 are equal to V_o .

It is obvious that the total flux change in the center leg (Φ_g) must be equal to zero within a half cycle. Define duty ratio D and period T as in Fig. 4. Phase $t_1 \sim t_2$ has time duration $(D - 0.5)T$; phase $t_2 \sim t_3$ has time duration $(1 - D)T$. By (2) and (4), $(D - 0.5)T \times (2V_i/N_p) + (1 - D)T \times ((2V_i/N_p) - (V_o/N_s)) = 0$.

The input-to-output voltage ratio is obtained

$$\frac{V_o}{V_i} = \frac{N_s}{N_p} \frac{1}{1 - D}. \quad (5)$$

B. Currents in Windings

Referring to the models in Fig. 4, in time duration $t_1 \sim t_2$

$$F_{p1} = F_{p2} = F_g (\text{Since } F_{j(j=1,2,3)} = 0). \quad (6)$$

From the definition of mmf

$$F_{p1} = N_{p1}I_{p1}, \quad F_{p2} = N_{p2}I_{p2}. \quad (7)$$

The input current is the summation of the currents in two primary windings

$$I_{in} = I_{p1} + I_{p2}. \quad (8)$$

From (6)–(8) and $N_{p1} = N_{p2} = N_p$

$$I_{in} = \frac{2F_g}{N_p}. \quad (9)$$

In time duration $t_2 \sim t_3$, the input current can also be expressed by (9). Actually, (9) is valid through the entire switching cycle. So, the input current is always proportional to the mmf on the gap. From Fig. 5, the average current through primary switch Q_1 or Q_2 is equal to $I_{in}/2$.

C. Magnetic Coupling

A feature of this circuit is that the input current is limited when the overlapping of two driving signals is small. This mechanism can be explained by comparing to its discrete core counterpart in Fig. 2 [10]. Fig. 7(a) shows the flux path of the auxiliary transformer T_2 . Fig. 7(b) shows the flux paths of the integrated magnetic transformer T when only switch Q_1 turns on.

In Fig. 7(a), winding turns $N_{d1} = N_{d2}$. Suppose the currents in the two windings are different, i.e., $I_{L1} = I_{L2} + \Delta I$. The difference current, ΔI , becomes the magnetizing current of transformer T_2 to generate the flux Φ . Subsequently ΔI is limited by the inductance of T_2 . In Fig. 7(b), since the reluctance of *Leg III* is much larger than the reluctance of *Leg II* due to the gap, most of the flux (Φ_2) goes through *Leg II*. Therefore, if the output voltage is high enough, the transformer exhibits large inductance to the input. The input current is then limited.

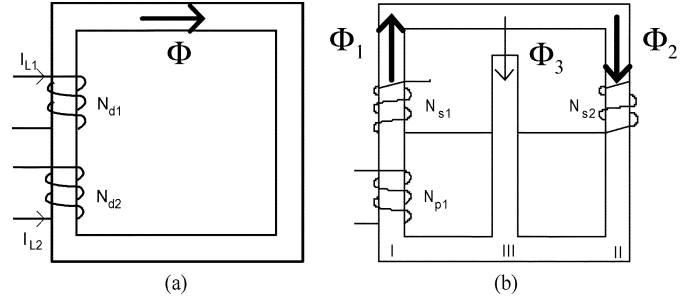


Fig. 7. Flux paths in the auxiliary transformer (T_2 in Fig. 2) and the integrated magnetic transformer (T in Fig. 3). (a) Flux path in T_2 of Fig. 2. (b) Flux paths in T of Fig. 3.

This explains the magnetic coupling mechanism of the proposed two-inductor boost converter.

It is important to note that the output voltage must be high enough, or, regulated. If the output voltage drops below the reflected input voltage, the transformer will directly deliver power to the load without inductor filtering. This problem is further discussed in Section V.

It can be seen in Fig. 3 that the topology splits the primary current into windings N_{p1} and N_{p2} . Topologies that split inductor current for buck mode converters are often referred to as current doublers [21]–[24], [28], [29]. In this case, however, the circuit in Fig. 3 is a boost topology, thus having completely different input-to-output voltage ratio, PWM control and driving strategies, windings consideration, start-up and protection circuit, etc. Moreover, an important issue in this boost application is how to limit the input power when the overlapping of two driving signals is small. This issue does not appear in buck mode current doublers [21]–[24], [28], [29].

III. TRANSFORMER DESIGN

When the design objectives such as input and output voltages, power level, tolerable input current ripple and peak flux density are given, the calculation may follow the steps below:

Step 1: Select the secondary-to-primary winding turns ratio $n = N_s/N_p$.

From (5), $n = (1 - D)(V_o/V_i)$. The minimum duty ratio for Boost mode operation is $D = 0.5$. The maximum duty ratio is typically determined by the controller and the number of start-up winding turns (which is discussed in Section V). The duty ratio range limits the selection of n .

Step 2: Select the magnetic core and the winding turns.

According to the power level and space requirements, a magnetic core can be tentatively selected. The number of primary and secondary winding turns N_p and N_s should be selected to achieve tolerable input current ripple and peak flux densities. The following formulas can be used to verify that the design values are within the tolerance. Detailed derivation is shown in the Appendix.

- *Input current ripple*

The peak-to-peak input current ripple can be derived as

$$I_{in-d} = \frac{2V_o(2D-1)(1-D)}{N_p N_s f_s P_g}. \quad (10)$$

The permeance of the gap P_g is defined by $P_g = \mu_0 A/l_g$ and is typically specified as the inductance factor (i.e., “ A_L ” value) in datasheets. f_s is the switching frequency; μ_0 is the permeability of air; A is the cross-sectional area of the gap; l_g is the gap length.

- *Peak flux density in the magnetic core*

The average flux density in the center leg is $B_{c-av} = N_p I_{in-av} P_g / (2A_c)$, where I_{in-av} is the average input current; A_c is the cross-sectional area of the center leg. The average flux density in the outer legs is (identical for two outer legs) $B_{o-av} = B_{c-av}/2$. The flux swing in the center leg is $B_{c-d} = 2V_o(1-D)(D-0.5)/(N_s f_s A_c)$. The flux swing in the outer legs is $B_{o-d} = V_o D(1-D)/(N_s f_s A_o)$, where A_o is the cross-sectional area of one outer leg.

Therefore, the peak flux density in the center leg is

$$B_{c-p} = B_{c-av} + \frac{B_{c-d}}{2}. \quad (11)$$

The peak flux density in the outer legs is

$$B_{o-p} = B_{o-av} + \frac{B_{o-d}}{2}. \quad (12)$$

Both B_{c-p} and B_{o-p} must be kept below the saturation value.

If one of the calculation results goes beyond the design target, the number of winding turn, core size or gap length is then adjusted. These quantities are calculated again until all the design specifications are satisfied.

IV. COMPARISON TO DISCRETE CORE BOOST TOPOLOGY

This section compares the magnetic assemblies in the boost circuit of Fig. 2 with the proposed integrated magnetic assembly in Fig. 3. The electrical stresses on the switches and the rectifiers are analyzed to be identical. Hence, the comparison focuses on the magnetic cores and their windings. To compare the sizes of magnetic cores, this section first derives the cross-sectional areas and the winding turns for each topology in terms of peak flux density and input current. Then, the size reduction of magnetic components due to integration is presented. Two assumptions are as follows.

Assumption 1: The electrical specifications are the same for both boost topologies.

Assumption 2: The cross-sectional area is determined based on the same peak flux densities.

Define: B_p —peak flux density; A_{dT1} —cross-sectional area of T_1 ; A_{dT2} —cross-sectional area of the auxiliary transformer; A_{dL} —cross-sectional area of each inductor; P_{dL} —permeance of the gap in each inductor; N_{au} —winding turns of T_2 ; N_{dp} —primary winding turn of T_1 ; N_{ds} —secondary winding turn of T_1 .

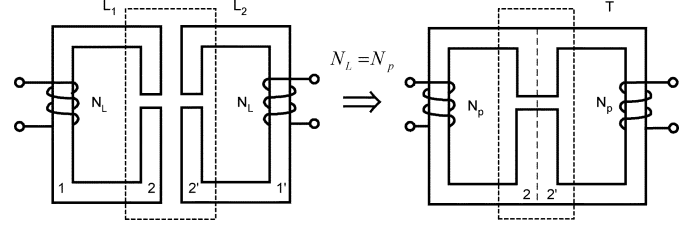


Fig. 8. Cross-sectional area comparison between two inductors and the center leg of the integrated magnetic transformer.

A. A_{dL} versus A_c

It is not difficult to derive

$$\frac{I_{in-av}}{2} + \frac{I_{in-d}}{4} = \frac{A_{dL} B_p}{N_L P_{dL}} = \frac{A_c B_p}{N_p P_g}. \quad (13)$$

Assumption 1 suggests that the input currents of two converters have identical ripples and average values. So, we can also obtain

$$2N_L^2 P_{dL} = N_p^2 P_g. \quad (14)$$

From (13) and (14), we have $2N_L A_{dL} = N_p A_c$. If we let $N_L = N_p$, then $2A_{dL} = A_c$. This result implies that if the inductor windings are used as the primary windings of the integrated magnetic transformer, the cross-sectional area of the center leg is equal to the combination of two inductors L_1 and L_2 side by side, as depicted in the dashed boxes of Fig. 8.

B. $A_{dT1} + A_{dT2}$ versus A_o

The peak fluxes in transformer T_1 and T_2 can be derived

$$A_{dT1} B_p = \frac{V_o(1-D)}{2N_{ds} f_s} \quad (15)$$

$$A_{dT2} B_p = \frac{V_o(1-D)}{2N_{ds} f_s} \cdot \frac{N_{dp}}{2N_{au}}. \quad (16)$$

The peak flux in the outer leg of the integrated magnetic core is

$$A_o B_p = \frac{1}{4} I_{in-av} N_p P_g + \frac{V_o(1-D)D}{2N_s f_s}. \quad (17)$$

Representing (15)–(17), in terms of input current ripple leads to

$$(A_{dT1} + A_{dT2}) B_p = \frac{N_L^2 P_{dL} I_{in-d}}{2(2D-1)N_{dp}} \left(1 + \frac{N_{dp}}{2N_{au}}\right) \quad (18)$$

$$A_o B_p = \frac{1}{4} N_p P_g \cdot \left(I_{in-av} + \frac{I_{in-d}}{2D-1} D\right). \quad (19)$$

To acquire an instructive comparison, it is reasonable to consider an example that satisfies a) $I_{in-d} = 20\% I_{in-av}$ and b) $N_{au} = N_{dp}$. Using (14), we can obtain the ratio

$$\frac{A_o}{A_{dT1} + A_{dT2}} = \frac{2(11D-5)N_{dp}}{3N_p}. \quad (20)$$

Ratio (20) is drawn in Fig. 9 for the duty ratio D varying between 0.5 and 1.

According to Fig. 9, depending on: 1) the winding turns of the isolation transformer, the auxiliary transformer and the induc-

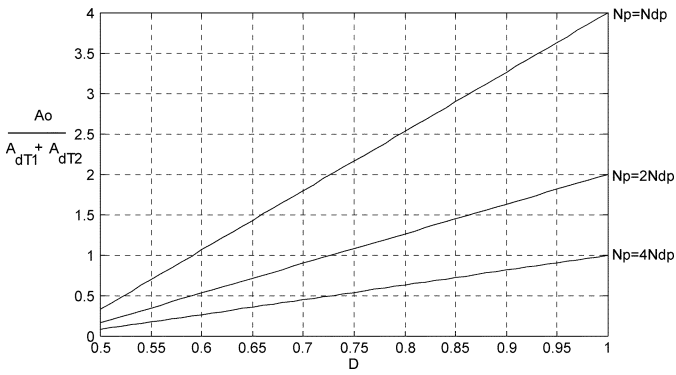


Fig. 9. Cross-sectional areas ratio between the outer leg of the integrated magnetic transformer and two discrete transformers T_1 and T_2 .

tors, 2) the current ripple requirement, and 3) steady state duty ratio, A_o can be larger or smaller than $A_{dT1} + A_{dT2}$. For example, if $N_p = 2N_{dp}$, when the designed duty ratio is less than 0.72, then $A_o < A_{dT1} + A_{dT2}$; otherwise, if the designed duty ratio is greater than 0.72, $A_o > A_{dT1} + A_{dT2}$. If $N_p = 4N_{dp}$, we always have $A_o < A_{dT1} + A_{dT2}$.

Two other considerations are as follows.

- 1) Suppose the input current ripple requirement is strict, i.e., $I_{in-d} \ll I_{in-av}$. Then by comparing (13) with (18) and (19), $2A_{dL}$ in the discrete core boost converter is expected to be larger than $A_{dT1} + A_{dT2}$. This is also true for A_c and A_o . Since in the discrete core boost converter, extra core legs (as *Leg I* and *Leg I'* in the inductors of Fig. 8) are needed to close the flux paths of the two inductors, the size reduction of the proposed integrated magnetic assembly can be justified.
- 2) The proposed magnetic assembly uses two primary windings. The number of winding turns is typically equal to that of the inductors. Therefore, the primary winding of T_1 and two windings of T_2 in Fig. 2 are saved. The fewer primary side windings and soldering connections reduce copper loss.

V. PRACTICAL CONSIDERATIONS

This section introduces two practical issues in two-inductor boost converters of both Figs. 2 and 3: start-up and protection. Solutions are provided to solve both issues by adding either one or two additional windings to the proposed magnetic assembly. Limitations of the solutions are also discussed.

A. Practical Issues

1) *Start-Up*: Before the circuit starts up, the output voltage is zero. If Q_1 and Q_2 begin to operate, the transformer-style coupling between the primary and secondary windings will deliver power directly from input to the load without inductor filtering. This is illustrated in Fig. 10. Suppose Q_2 is off and Q_1 turns on. Since the center leg exhibits large reluctance, most flux flows through *Leg II*. The voltages on N_{s1} and N_{s2} have the polarities as indicated in Fig. 10. The large initial current may damage the

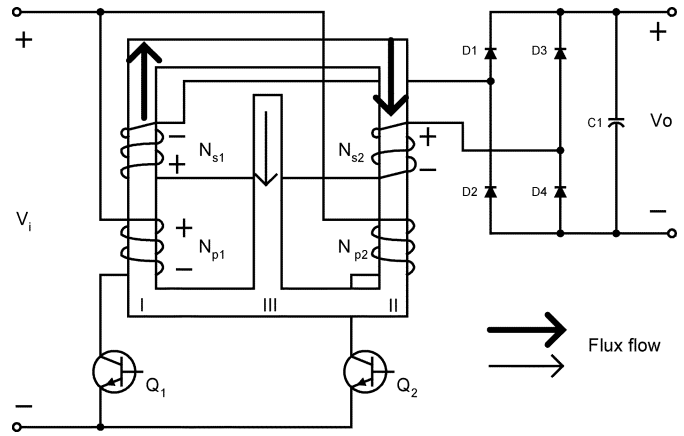


Fig. 10. Circuit start-up problem.

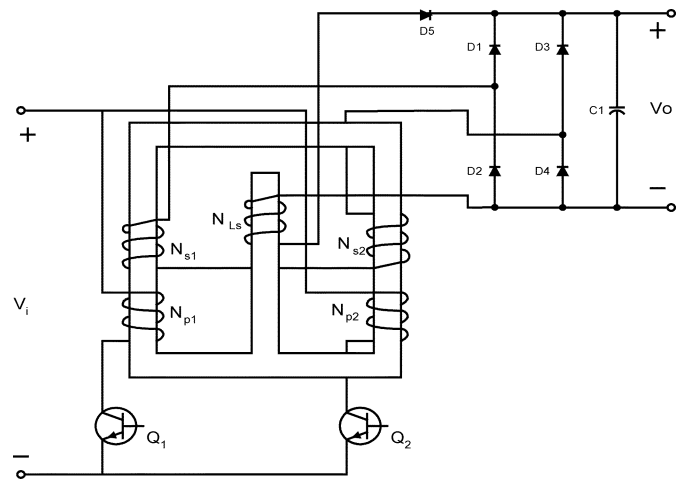


Fig. 11. Circuit with one additional winding.

semiconductor devices in the current path. Therefore, the output capacitor must be pre-charged in advance to block the diodes.

2) *Protection*: Even when employing a protection mechanism in the control unit, occasional duty ratio error ($D < 0.5$) may occur. This will damage the converter because there is no path to release the energy in the gap if both switches turn off.

B. Solution

Several start-up schemes have been proposed for boost type isolated topologies [25], [26]. A typical solution is to add a flyback transformer on the primary side. However, this means that another magnetic component is required. This section proposes a solution that can be used for both start-up and protection purposes. Fig. 11 shows the proposed solution by adding one additional winding N_{Ls} around the center leg. Fig. 12 shows the solution by adding two additional windings N_{Ls1} and N_{Ls2} around two outer legs, respectively.

1) *Start-Up*: The circuit in Fig. 12 is used to illustrate the operating principle. The operating waveforms are shown in Fig. 13. The driving signals of Q_1 and Q_2 are identical. The circuit is operating in flyback mode. As in Fig. 14, when Q_1 and Q_2 turn on (stage 1), the flux is stored in the gap and none of the secondary side windings conduct. When Q_1 and Q_2 turn off (stage 2), the additional windings deliver the stored

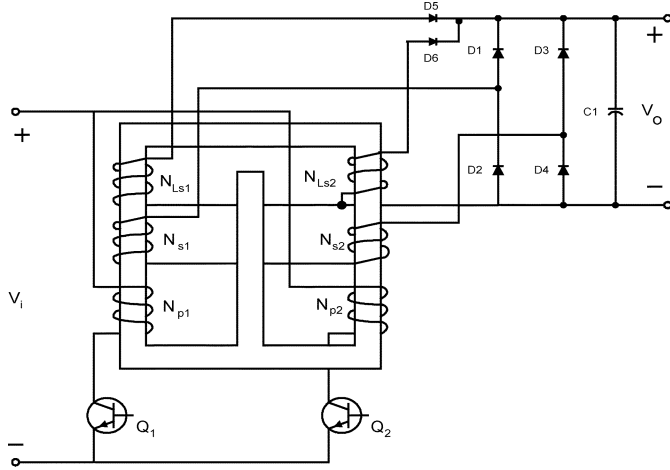


Fig. 12. Circuit with two additional windings.

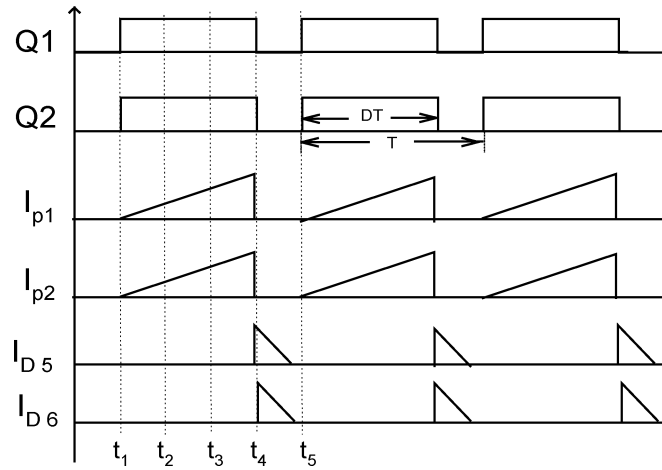


Fig. 13. Operating waveform of start-up circuit.

energy in the gap to the output. In both stages, $D_1 - D_4$ are blocked because the overall voltage between two terminals of the secondary windings is zero. Indeed, the primary windings N_{p1} , N_{p2} and the additional windings N_{Ls1} and N_{Ls2} form an integrated magnetic push-pull circuit [27]. However, this circuit cannot work in Buck mode (i.e., Q_1 and Q_2 cannot be closed alternatively) because it will also cause the direct power transfer from the primary windings to the secondary windings without filtering inductance.

In normal boost mode operation, the lowest output voltage appears when duty ratio $D = 0.5$. By (5), the minimum charged voltage V_{o_pre} should satisfy $V_{o_pre} \geq 2(N_s/N_p)V_i$.

2) *Protection*: When both primary switches turn off, these additional windings provide current paths for releasing the energy from the gap. The energy is sent to the secondary side, as in Stage 2 of the start-up mode. Therefore, the additional windings can also be used for protection against occasional duty ratio error.

To avoid interfering with the normal operation, the maximum duty ratio is limited by the additional windings. Referring to the circuit in Fig. 11, in operation phase $t_1 \sim t_2$, the direction of flux rate in the center leg is downward, as in Fig. 4. The reflected voltage on the inductor winding blocks D_5 . However, in operation phase $t_2 \sim t_3$, the flux flow in the center

leg attempts to forward bias D_5 . To avoid this, the reflected voltage on N_{Ls} must be lower than the output voltage. Therefore, $((V_o/N_s) - (2V_i/N_p)) \times N_{Ls} < V_o$. By (5), the constraint on the inductor winding turn is $N_{Ls} < N_s/(2D_{max} - 1)$. For the same reason, the windings N_{Ls1} and N_{Ls2} in Fig. 12 should satisfy $N_{Ls1} < N_s/D_{max}$, $N_{Ls2} < N_s/D_{max}$.

An alternative protection scheme is to build an additional clamping circuit. However, since the additional windings can be used for protection, the extra circuit is only necessary to absorb the energy in the leakage inductance. Specifically, let the leakage inductance be L_{lk} and peak input current I_{in-p} . Since each primary switch conducts half of the input current at the time it is turned off, the leakage energy in the primary winding is $(1/8)L_{lk}I_{in-p}^2$, which cannot be dissipated through added secondary windings. To limit the voltage spike on the primary switches, a clamping circuit may be used.

VI. TOPOLOGY VARIATIONS

Two topology variations are shown in Figs. 15 and 16. Fig. 15 implements the two-inductor boost converter by using a magnetic core with two gaps in two outer legs. The secondary winding is center tapped. The rectification stage can use full-wave instead of full-bridge structure. This saves two output rectifiers. However, the two current paths on the primary side are not coupled. It loses the advantage of wide power regulation range.

Fig. 16 inserts an additional inductor winding N_{Lp} around the center leg compared with the transformer in Fig. 3. The inductor winding is inserted between the input and the connection of two primary windings. N_{Lp} does not change the input-to-output voltage ratio but influences the primary current ripple and the flux distribution in three core legs. To reduce the primary copper loss, the two primary windings typically have minimum number of winding turns. Hence, the primary inductance may not be large enough to maintain low input current ripple. The added inductor winding enhances the primary filter inductance. This is desirable in some applications in which the optimization of the transformer is crucial. A general explanation of the theory and the advantages of adding a winding on the center legs of integrated magnetic circuit are introduced in [28], [29].

VII. SIMULATION AND EXPERIMENTAL RESULTS

Although this topology is better suited for high power application, the experiment was implemented on a 40-W level. (The low power level was selected due to academic lab facility limitations.) The design specifications are: input voltage: 2.5 V; output voltage: 72 V; maximum input current ripple 5 A. The circuit is shown in Fig. 17. The driving scheme is selected by the output voltage. If the output voltage is below the designed pre-charge voltage, the PWM control unit works in start-up mode. If the output voltage is high enough, the PWM control unit switches to boost mode.

The circuit is operating at switching frequency 170 kHz. Three-paralleled Si4466 are used as the primary switches. The turns ratio of the transformer is selected as 12. According to the power level, one E18/4/3F3 magnetic core was used with $A_L = 250$ nH. From design criteria (10)–(12), $N_p = 2$ can satisfy the

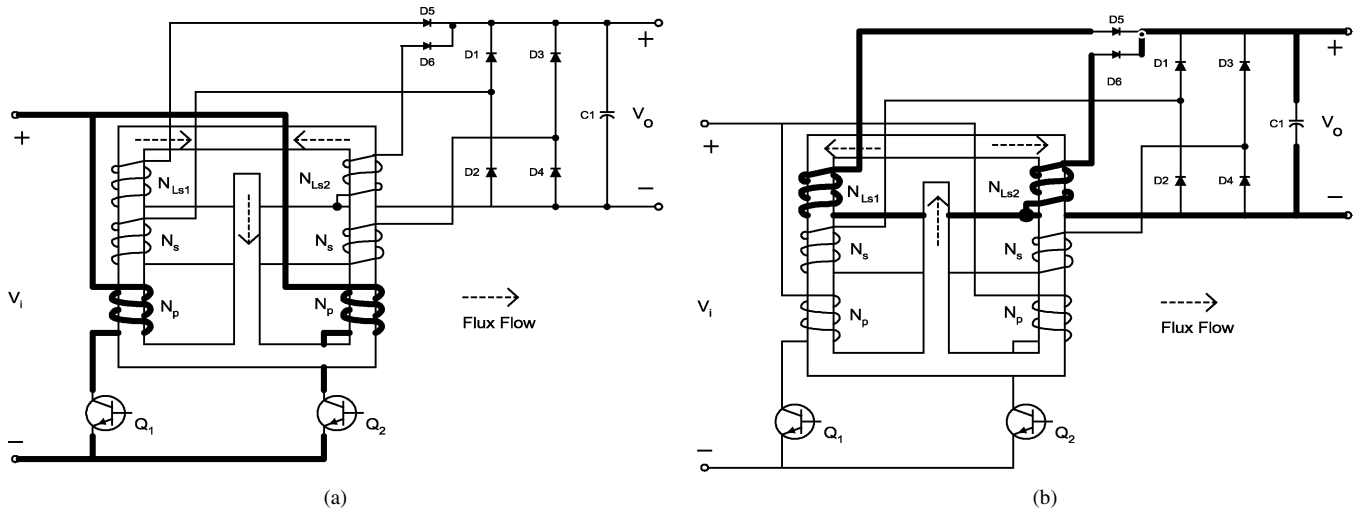


Fig. 14. Operating stages of start-up circuit: (a) Stage 1 and (b) Stage 2.

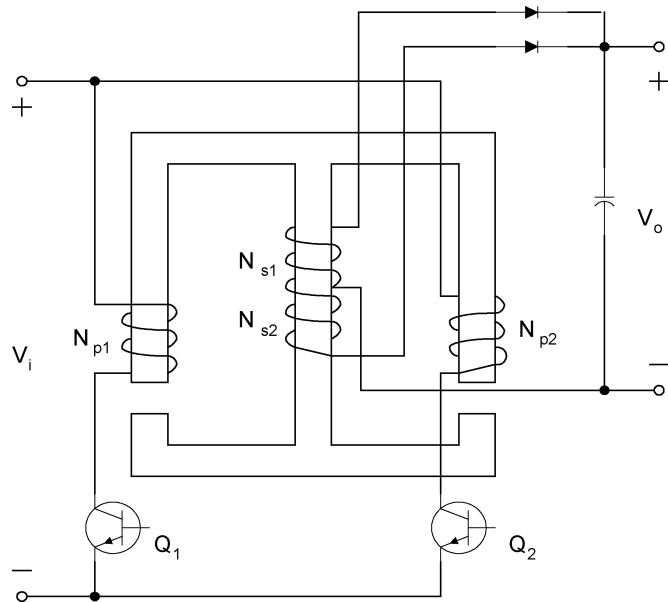


Fig. 15. Two gaps implementation.

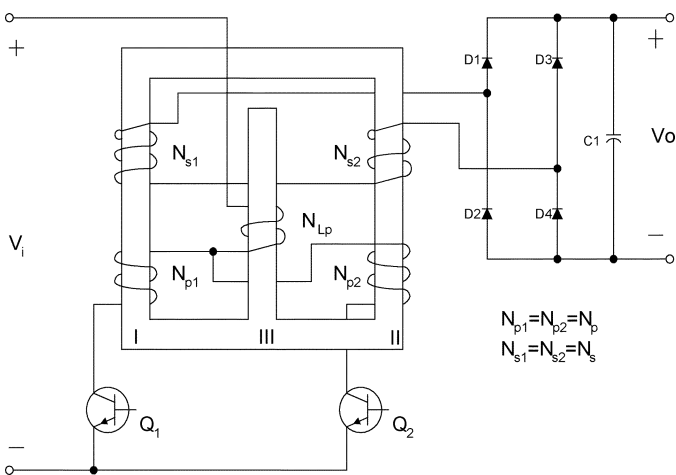


Fig. 16. Additional inductor winding.

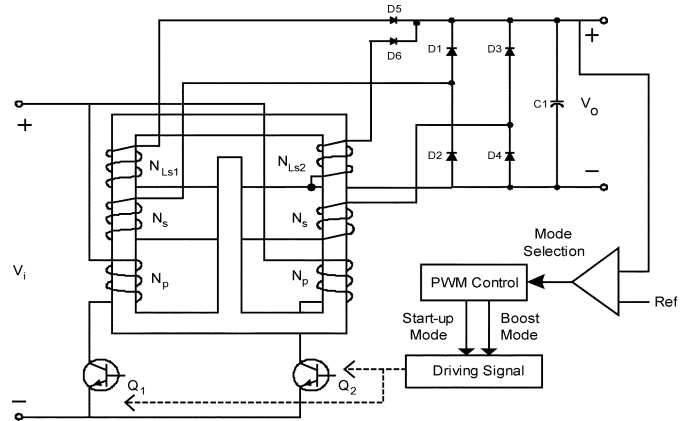


Fig. 17. Simulation and experimental circuit.

above requirements and also provide sufficient duty ratio range for regulation. The secondary winding N_s is then 24 turns. The flux densities in the core are: Peak flux density in the center leg is 106 mT; Peak flux density in the outer legs is 199 mT.

The simulation and experimental results are shown in Fig. 18–20. Fig. 18 shows the start-up waveform. From the current waveforms of D_5 and D_6 , it is obvious that the circuit is operating in flyback mode. Fig. 19 shows the normal operating waveform when the circuit is operating in boost mode. The output power is 36 W. The results are consistent with the analysis of the operating principle. That is, in the boost-operating mode, the input current only increases when both switches Q_1 and Q_2 are closed. Fig. 20 shows the operating waveform when the load is light—2 W. The input current goes to zero before the driving signal changes. It indicates that when the output current is small, the circuit works at discontinuous mode. This result verifies the analysis that the integrated magnetic boost converter removes the limitation of power regulation range in the original circuit of Fig. 1.

VIII. CONCLUSION

An integrated magnetic isolated two-inductor boost converter is presented. The converter is implemented by using a single

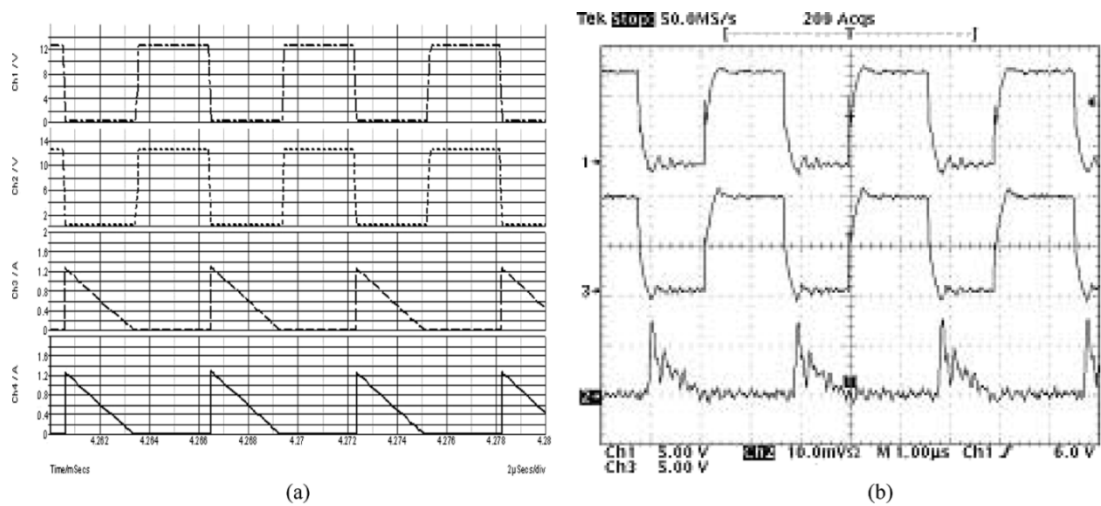


Fig. 18. Start-up mode. (a) Simulation: start-up mode (Ch1, Ch2: driving signals; Ch3: current in diode D5; Ch4: current in diode D6.). (b) Experiment: start-up mode (Ch1, Ch3, driving signals; Ch2: current in D5, 500 mA/DIV).

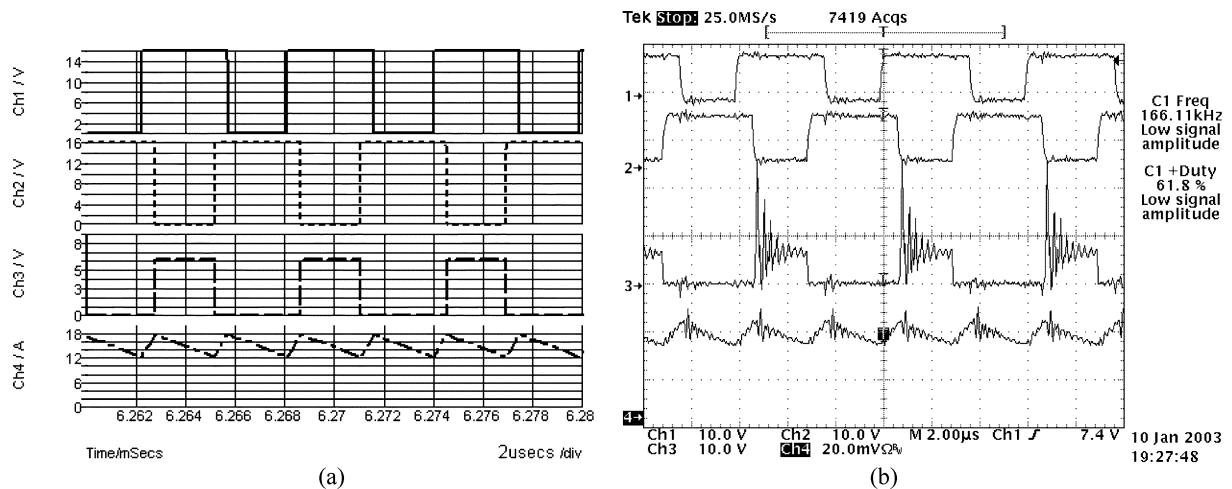


Fig. 19. Boost mode, output power 36 W. (a) Simulation: boost mode (Ch1, Ch2: driving signals; Ch3: drain-source voltage of Q2; Ch4: input current.). (b) Experiment: boost mode (Ch1, Ch2: driving signals; Ch3: drain-source voltage on Q2; Ch4: input current, 10 A/DIV).

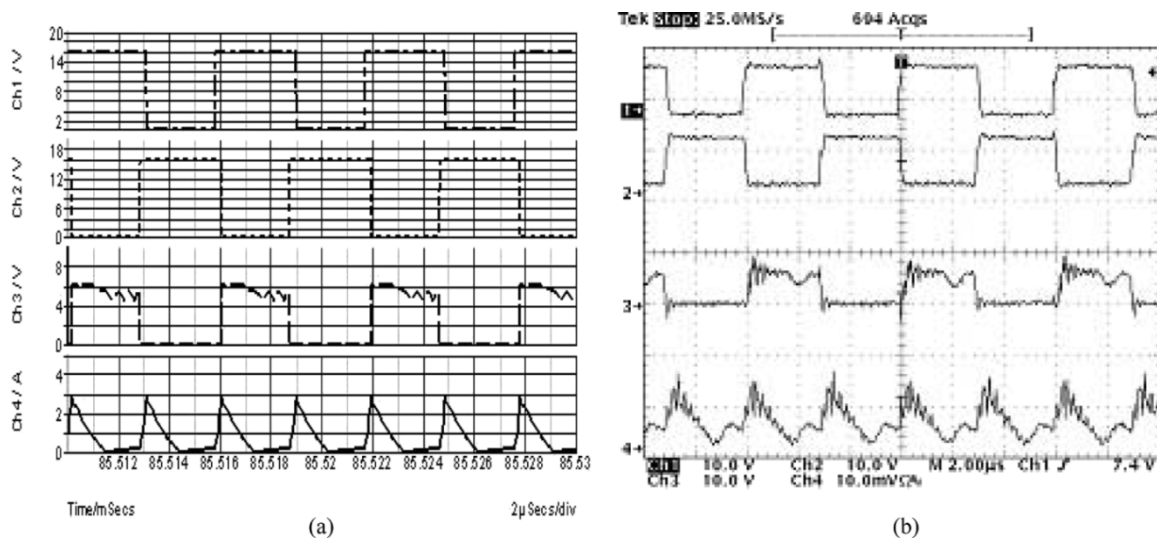


Fig. 20. Boost mode, output power 2 W. (a) Simulation: boost mode (Ch1, Ch2: driving signals; Ch3: drain-source voltage of Q2; Ch4: input current.). (b) Experiment: boost mode (Ch1, Ch2: driving signals; Ch3: drain-source voltage on Q2; Ch4: input current, 2 A/DIV).

magnetic core with one gap in the center leg. Two inductor windings are intrinsically coupled. Experimental and simulation results verify the operating principle. Practical implementation issues including start-up and protection are solved. The proposed topology maintains wide power regulation range. Some advantages of the proposed integrated magnetic core topology over the discrete magnetic core solution include: reduction in the number of magnetic assemblies; reduction in the number of windings on the primary side of the circuit; and hence reduction in the number of soldering connections on the primary side. Furthermore, as explained in this paper, by careful design, the volume of the magnetic material may also be reduced.

APPENDIX FORMULA DERIVATION

Consider the circuit in Fig. 3 of the proposed integrated magnetic assembly. This Appendix derives the input current ripple and the flux densities in the core.

A. Input Current Ripple

In time duration $(1 - D)T$, the flux rate in the center leg is given by (4). The flux change in the gap is then $\Phi_{g-d} = ((V_o/N_s) - (2V_i/N_p))(1 - D)T$. From (9), we have $N_p I_{in-d} = 2F_{g-d}$. Since $F_{g-d} = \Phi_{g-d}/P_g$, the input current ripple is given as

$$I_{in-d} = \frac{2V_o(2D - 1)(D - 0.5)}{N_p N_s f_s P_g}. \quad (21)$$

B. Average Flux Density in the Center Leg

The average mmf on the gap is calculated as $F_{g-av} = B_{c-av} A_c / P_g$. From (9), $N_p I_{in-av} = 2F_{g-av}$. So, the average flux density in the center leg is

$$B_{c-av} = \frac{N_p I_{in-av} P_g}{2A_c}. \quad (22)$$

C. Flux Swing in the Center Leg

In time duration $(D - 0.5)T$, the flux rate in the center leg is given by (2). From (2) and (5), $\dot{\Phi}_3 = (2V_o/N_s)(1 - D)$. The flux change in the center leg: $\Phi_{c-d} = (2V_o(1 - D)(D - 0.5)/N_s f_s)$. Therefore, the flux density swing is

$$B_{c-d} = \frac{2V_o(1 - D)(D - 0.5)}{N_s f_s A_c}. \quad (23)$$

D. Flux Swing in the Outer Leg

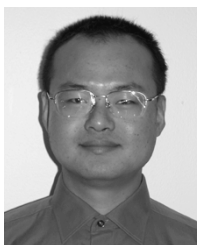
During time duration DT of switch Q_1 , from (1) and (3), the flux rate in Leg I is $\dot{\Phi}_1 = V_i/N_p$, or $\dot{\Phi}_1 = V_o/N_s(1 - D)$. The flux change is $\Phi_{o-d} = V_o D(1 - D)/N_s f_s$. The flux density swing is then

$$B_{o-d} = \frac{V_o D(1 - D)}{N_s f_s A_o}. \quad (24)$$

REFERENCES

- [1] B. A. Miwa, D. M. Otten, and M. F. Schlecht, "High efficiency power factor correction using interleaving techniques," in *Prloc. IEEE APEC'92 Conf.*, 1992, pp. 557–568.
- [2] J. W. Kolar, G. R. Kamath, N. Mohan, and F. C. Zach, "Self-adjusting input current ripple cancellation of coupled parallel connected hysteresis-controlled boost power factor correctors," in *Proc. IEEE PESC'95 Conf.*, 1995, pp. 164–173.
- [3] M. S. Elmore, "Input current ripple cancellation in synchronized, parallel connected critically continuous boost converters," in *Proc. IEEE APEC'96 Conf.*, 1996, pp. 152–158.
- [4] J. R. Pinheiro, H. A. Grundling, D. L. R. Vidor, and J. E. Baggio, "Control strategy of an interleaved boost power factor correction converter," in *Proc. IEEE PESC'99 Conf.*, 1999, pp. 137–142.
- [5] H. A. C. Braga and I. Barbi, "A 3-kW unity-power-factor rectifier based on a two-cell boost converter using a new parallel-connection technique," *IEEE Trans. Power Electron.*, vol. 14, no. 1, pp. 209–217, Jan. 1999.
- [6] B. T. Irving, Y. Jang, and M. M. Jovanovic, "A comparative study of soft-switched CCM boost rectifiers and interleaved variable-frequency DCM boost rectifier," in *Proc. IEEE APEC'00 Conf.*, 2000, pp. 171–177.
- [7] A. V. D. Bossche, V. Valtchev, J. Ghijselen, and J. Melkebeek, "Two-phase zero-voltage switching boost converter for medium power applications," in *Proc. IEEE Industry Applications Soc. Annu. Meeting*, New Orleans, LA, 1998, pp. 1546–1553.
- [8] P. J. Wolfs, "A current-sourced dc-dc converter derived via the duality principle from the half-bridge converter," *IEEE Trans. Ind. Electron.*, vol. 40, no. 1, pp. 139–144, Feb. 1993.
- [9] M. T. Zhang, Y. Jiang, F. C. Lee, and M. M. Jovanovic, "Single-phase three-level boost power factor correction converter," in *Proc. IEEE APEC'95 Conf.*, 1995, pp. 434–439.
- [10] G. Ivensky, I. Elkin, and S. Ben-Yaakov, "An isolated dc/dc converter using two zero current switched IGBT's in a symmetrical topology," in *Proc. IEEE PESC'94 Conf.*, 1994, pp. 1218–1225.
- [11] Y. Jang and M. M. Jovanovic, "New two-inductor boost converter with auxiliary transformer," in *Proc. IEEE APEC'02 Conf.*, 2002, pp. 654–660.
- [12] Y. Jang and M. M. Jovanovic, "Two-Inductor Boost Converter," U.S. Patent 6 239 584, May 29, 2001.
- [13] E. Bloom, "New integrated-magnetic dc-dc power converter circuits & systems," in *Proc. IEEE APEC'87 Conf.*, 1987, pp. 57–66.
- [14] R. Severns and E. Bloom, *Modern DC/DC Switchmode Power Converter Circuits*. New York: Van Nostrand Reinhold, Dec. 1985.
- [15] E. Bloom, "Core selection for & design aspects of an integrated-magnetic forward converter," in *Proc. IEEE APEC'86 Conf.*, 1986, pp. 141–150.
- [16] D. K. Cheng, L. Wong, and Y. S. Lee, "Design, modeling, and analysis of integrated magnetics for power converters," in *Proc. IEEE PESC'00 Conf.*, 2000, pp. 320–325.
- [17] D. C. Hamill, "Lumped equivalent circuits of magnetic components: the gyrator-capacitor approach," *IEEE Trans. Power Electron.*, vol. 8, no. 2, pp. 97–103, Apr. 1993.
- [18] D. C. Hamill, "Gyrator-capacitor modeling: a better way of understanding magnetic components," in *Proc. IEEE APEC'94 Conf.*, 1994, pp. 326–332.
- [19] L. Yan and B. Lehman, "Better understanding and synthesis of integrated magnetics with simplified gyrator model method," in *Proc. IEEE PESC'01 Conf.*, 2001, pp. 433–438.
- [20] M. E. Eaton, "Adding flux paths to SPICE's analytical capability improves the ease and accuracy of simulating power circuits," in *Proc. IEEE APEC'98 Conf.*, 1998, pp. 386–392.
- [21] O. S. Seiersen, "Power supply circuit with integrated magnetic components," U.S. Patent 5 335 163, Aug. 2, 1994.
- [22] G. Q. Morris, "Magnetically integrated full wave dc to dc converter," U.S. Patent 5 555 494, Sep. 10, 1996.
- [23] W. Chen, "Single magnetic low loss high frequency converter," U.S. Patent 5 784 266, Jul. 21, 1998.
- [24] P. Xu, Q. Wu, P. Wong, and F. C. Lee, "A novel integrated current doubler rectifier," in *Proc. IEEE APEC'00 Conf.*, 2000, pp. 735–740.
- [25] L. Zhu, K. Wang, F. C. Lee, and J. Lai, "New start-up schemes for isolated full-bridge boost converters," in *Proc. IEEE APEC'00 Conf.*, 2000, pp. 309–313.

- [26] L. Zhu, K. Wang, F. C. Lee, and J. Lai, "New start-up schemes for isolated full-bridge boost converters," *IEEE Trans. Power Electron.*, vol. 18, no. 4, pp. 946–951, Jul. 2003.
- [27] F. Barthold, "Full wave buck-boost power converter with buck power converter properties," U.S. Patent 5 436 818, Jul. 25, 1995.
- [28] L. Yan, D. Qu, and B. Lehman, "Integrated magnetic full wave converter with flexible output inductor," *IEEE Trans. Power Electron.*, vol. 18, no. 2, pp. 670–678, Mar. 2003.
- [29] J. Sun, K. F. Webb, and V. Mehrotra, "An improved current-doubler rectifier with integrated magnetics," in *Proc. IEEE APEC'02 Conf.*, 2002, pp. 831–837.



Liang Yan (S'04) received the B.E. and M.E. degrees from Shanghai Jiaotong University, Shanghai, China, in 1995 and 1998, respectively, and the Ph.D. degree in electrical engineering from Northeastern University, Boston, MA, in 2004.

From 1998 to 1999, he worked for Huawei Electrical Inc., Shenzhen, China. He is currently working for MKS ENI Products, Rochester, NY.



Brad Lehman (M'92) received the B.E.E. degree from the Georgia Institute of Technology, Atlanta, in 1987, the M.S.E.E. degree from the University of Illinois at Champaign-Urbana, in 1988, and the Ph.D. degree in electrical engineering from the Georgia Institute of Technology, Atlanta, in 1992.

He is presently an Associate Professor in the Department of Electrical and Computer Engineering, Northeastern University, Boston, MA, and previously was a Hearin Hess Distinguished Assistant Professor at Mississippi State University, Mississippi

State, MS. He was previously an NSF Presidential Faculty Fellow, and also a Visiting Scientist at the Massachusetts Institute of Technology, Cambridge. He performs research in the areas of power electronics, electric motor drives, and control. A primary focus of his research is in the modeling, design and control of dc–dc converters.

Dr. Lehman received the Alcoa Science Foundation Fellowship. He is an Associate Editor of the *IEEE TRANSACTIONS ON POWER ELECTRONICS*, and from 1993 to 1997, served as an Associate Editor for the *IEEE TRANSACTIONS ON AUTOMATIC CONTROL*.